CrystEngComm

View Online / Journal Homepage
Dynamic Article Links

Cite this: DOI: 10.1039/c2ce06270d

www.rsc.org/crystengcomm

PAPER

Solution synthesis of copper selenide nanocrystals and their electrical transport properties†

Guanjun Xiao,[a] Jiajia Ning,[a] Zhaoyang Liu,[b] Yongming Sui,[a] Yingnan Wang,[a] Qingfeng Dong,[b] Wenjing Tian,*[b] Bingbing Liu,[a] Guangtian Zou[a] and Bo Zou*[a]

Received 26th September 2011, Accepted 23rd November 2011
DOI: 10.1039/c2ce06270d

In this paper, we developed a one-pot solution strategy to synthesize copper selenide NCs with controllable shape and structure. By changing the precursors in the reaction, copper selenide NCs ($Cu_{2-x}Se$ nanoparticles, nanorods and CuSe nanoplates) with various morphologies could be achieved. We proposed a possible mechanism to explain the influence of precursors on the shape of copper selenide NCs and we found that the chemical activities of precursors played key roles in the morphologies and crystal structures of the final products. Moreover, the electrical transport properties of as-prepared products were investigated. The morphologies of copper selenide NCs have a great influence on the electrical transport properties. The copper selenide NCs with nanorods display the best electrochemical performance compared with the other two types. We believe that copper selenide NCs would be promising candidates for electrical transport materials.

1 Introduction

During the past decades, chalcogenide semiconductor nanocrystals (NCs) have attracted broad attention due to their unique shape- and size-dependent physical and chemical properties that differ drastically from their bulk counterparts.[1–5] The shape and size of inorganic NCs play a crucial role in determining their basic properties[6] and potential applications in nano-electronic devices, nano-optical devices and sensors,[7] *etc.* A series of semiconductor NCs with various shape and size have been obtained. Among the entire semiconductor NCs, metal-selenide NCs occupy an important position in both fundamental science and technological applications.[8–14] Particularly, copper selenide is a significant p-type I–VI semiconductor, which is a promising candidate for solar cells,[15] gas sensors,[16] super ionic conductors[17] and thermoelectric converters.[18] Moreover, CuSe was demonstrated to be a good precursor for fabricating chalcopyrite $CuInSe_2$-based nanostructures on a large scale.[19] Because of the importance of copper selenide to materials science, extensive efforts have been devoted to synthesizing copper selenide NCs with various shape and size. CuSe quantum dots, Cu_3Se_2 nanoplates, CuSe nanotubes and $Cu_{2-x}Se$ nanocubes and their corresponding hierarchical nanodendrites have been produced by thermolysis of single-source precursor,[20] ultrasonochemical techniques,[21,22] template-directed reaction,[23] an electrochemical crystallization process,[24] and a hydrothermal method,[25,26] respectively. Recently, $Cu_{2-x}Se$ nanoparticles have been produced *via* a hot-injection method, which used relatively unstable and air sensitive CuCl at a relatively high temperature.[27]

However, how to develop a synthetic route to prepare the nanomaterials, including copper selenide NCs with desired morphologies and structures, remains an endless pursuit in materials physics and synthetic chemistry. Solution routes are attractive alternative strategies for synthesizing the nanocrystals, due to their morphology-controlling capability and easy preparation of films for device fabrication, which have been used to fabricate noble metal NCs, metal oxides NCs, and semiconductor NCs.[28–32] In the present work, we describe an environmentally friendly one-pot solution route to synthesize high-quality copper selenide NCs with controllable shape and structure. The as-prepared copper selenide NCs with various shapes and structures were obtained template-free at a relatively moderate temperature and limited time in comparison with the previous reports.[23,27] Generally, the non-injection approach is much more reproducible and ready to scale up than the hot-injection method, avoiding the high-temperature process.[33] Furthermore, we discussed the influence of precursors on the shape and structure of copper selenide NCs and it is proved that the chemical activities of precursors in the reaction system have played key roles in the resulting products. To further evaluate the potential device applications with copper selenide NCs, we systematically investigated the electrical properties based on the copper selenide NCs with controllable shape and structure; meanwhile, the rational reasons for the different performances dependent on the morphologies were interpreted. The excellent performance of copper selenide NCs

[a]*State Key Laboratory of Superhard Materials, Jilin University, Changchun, 130012, China. E-mail: zoubo@jlu.edu.cn*
[b]*State Key Laboratory of Supramolecular Structure and Materials, Jilin University, Changchun, 130012, China. E-mail: wjtian@jlu.edu.cn*
† Electronic supplementary information (ESI) available. See DOI: 10.1039/c2ce06270d

as electron transport materials may open new opportunities for device applications.

2 Experimental sections

2.1 Chemicals

Copper(II) acetylacetonate ($Cu(acac)_2$, ≥99.99%), copper(II) acetate ($Cu(Ac)_2$, 99.999%), selenium (Se, 99.95+%), oleic acid (OA, 90%) and 1-octadecene (ODE, 90%) were purchased from Aldrich. Oleylamine (OLA, ≥70%) was purchased from Fluka. Selenourea ($SeC(NH_2)_2$, 99.9+%) was purchased from Alfa Aesar. Selenium dioxide (SeO_2, ≥99.0%) was purchased from Tianjin Damao Chemical Reagent Factory. Toluene, methanol, chloroform and acetone, which were analytical grade, were purchased from Beijing Chemical Company. All chemicals used in the experiments were without further purification.

2.2 Synthesis

a) Synthesis of cubic $Cu_{2-x}Se$ nanoparticles. Typically, $Cu(acac)_2$ (0.2 mmol), $SeC(NH_2)_2$ (0.2 mmol) and OLA (10 mL) were loaded into a 50 mL three-neck flask in a glove box. Then the flask was sealed and taken out to connect to the Schlenk line equipped with a condenser. The equipment was heated to 200 °C under a nitrogen flow and vigorous magnetic stirring conditions. When the temperature was up to 200 °C, the subsequent dark green reaction mixture was stirred for an additional 10 min. The samples were collected by centrifugation with toluene and methanol (1 : 1 by volume ratio) several times.

b) Synthesis of cubic $Cu_{2-x}Se$ nanorods. Similar to that of $Cu_{2-x}Se$ nanoparticles, 0.2 mmol of $Cu(Ac)_2$ and 0.2 mmol of SeO_2 were employed as precursors, 2 mL of OA and 8 mL of ODE were used as ligand and solvent, respectively. When the temperature was up to 200 °C, the dark black reaction mixture was stirred for an additional 10 min. The products were isolated by centrifugation with chloroform and acetone (<1 : 1 by volume ratio) several times.

c) Synthesis of hexagonal CuSe nanoplates. The only difference was that 0.2 mmol of $Cu(Ac)_2$ and 0.2 mmol of Se were substituted as reagents. When the temperature was up to 200 °C, the dark gray reaction mixture was stirred for an additional 10 min. The samples were precipitated by centrifugation with toluene and methanol (1 : 1 by volume ratio) several times.

2.3 Characterization

An X-ray powder diffractometer (Shimadzu, XRD-6000) operating at 40 kV and 40 mA with Cu-Kα radiation was used to record the X-ray diffraction (XRD) patterns of the samples. Data were collected from 20–80° with a sampling interval of 0.02° per step and a scan speed of 4° per minute. Transmission electron microscopy (TEM) images were obtained in a Hitachi H-8100IV transmission electron microscopy using an acceleration voltage of 200 kV. High resolution transmission electron microscopy (HRTEM) images and selected area electron diffraction (SAED) pattern were measured *via* a JEM-2100 transmission electron microscopy at 200 kV. Samples for TEM were prepared on copper grid by drop-casting toluene solution of the nanomaterials. Ultraviolet-visible absorption (UV-vis) spectra were performed by a Shimadzu UV-3150 spectrometer. Photoluminescence (PL) emission spectra were carried out *via* Photon Technology International Company equipment.

For device fabrication, the ITO glass was pre-cleaned and copper selenide NCs were spin-coated onto the ITO from chloroform solution, the thickness of films was measured by Veeco DEKTAK 150 surface profilometer. The devices were completed by evaporating a 100 nm of Al at a base pressure of 5×10^{-4} Pa. The effective area as defined by the geometrical overlap between the bottom ITO electrode and the Al electrode was 5 mm^2. The *I–V* characteristics were recorded from −6 to 6 V by using Keithley 2400 Source Meter. All fabrication and characterizations were performed in an ambient environment.

3 Results and discussion

The crystal structure and chemical composition of as-prepared samples were confirmed by powder X-ray diffraction (XRD). Fig. 1 shows the XRD patterns of as-prepared copper selenide NCs. As shown in Fig. 1a and 1b, all the diffraction peaks can be indexed to cubic crystal structure $Cu_{2-x}Se$ (JCPDS No. 06-0680), and obvious diffraction peaks can be indexed to (111) (200) (220) (311) (400) and (331) planes of cubic crystal structure $Cu_{2-x}Se$. The weak and wide diffraction peaks are responding to the smaller size of $Cu_{2-x}Se$ NCs (Fig. 1a). XRD pattern in Fig. 1c is responding to hexagonal crystal structure CuSe, which are in good agreement with the standard JCPDS card No. 34-0171. All the diffraction peaks are according to (101) (102) (006) (110) (108) (116) and (208) planes of hexagonal crystal structure CuSe, respectively. No other diffraction peaks appear, indicating the samples are pure $Cu_{2-x}Se$ or CuSe.

Copper selenide NCs with different shapes and structures were prepared by changing precursors in the synthetic system. Transmission electron microscopy (TEM) images and the structural models of copper selenide NCs are shown in Fig. 2.

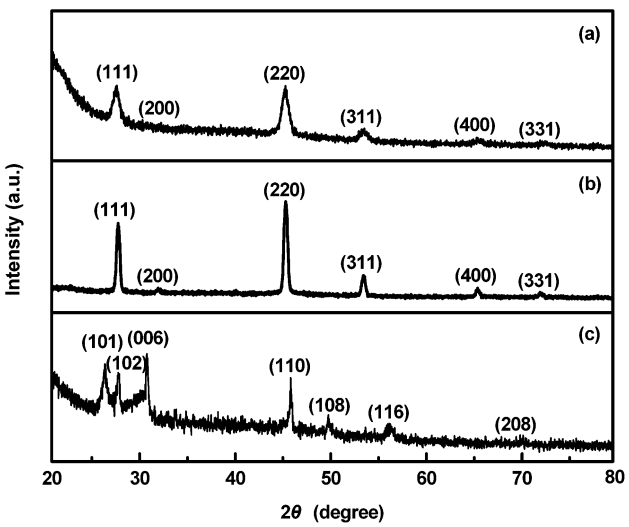

Fig. 1 X-ray diffraction (XRD) patterns of the as-prepared copper selenide NCs. (a) $Cu_{2-x}Se$ nanoparticles, (b) $Cu_{2-x}Se$ nanorods and (c) CuSe nanoplates.

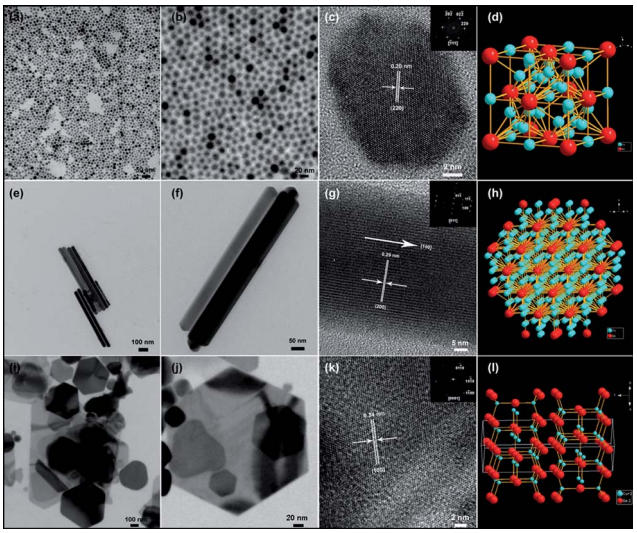

Fig. 2 Transmission electron microscopy (TEM) images and structural models of copper selenide NCs. (a)–(c) TEM images with different magnification and HRTEM image of $Cu_{2-x}Se$ nanoparticles, (d) the unit cell of face-centered cubic $Cu_{2-x}Se$ NCs, (e)–(g) TEM images with different magnifications and HRTEM of $Cu_{2-x}Se$ nanorods, (h) molecular structure of face-centered cubic $Cu_{2-x}Se$ NCs, (i)–(k) TEM images with different magnification and HRTEM of CuSe nanoplates, (l) the molecular structure of hexagonal CuSe NCs, insets of (e), (g) and (k) are fast Fourier transform (FFT) patterns of the copper selenide NCs HRTEM imaged in corresponding (e),(g) and (k).

Fig. 2a–c represent TEM images and high resolution transmission electron microscopy (HRTEM) image of $Cu_{2-x}Se$ nanoparticles. Nearly monodisperse nanoparticles with size of 12 nm were obtained. The size distribution shown in Fig. 3 indicates that $Cu_{2-x}Se$ nanoparticles are highly uniform with a standard deviation σ of 2.8 nm. HRTEM image of an individual nanoparticle is given in Fig. 2c, we can see that $Cu_{2-x}Se$ nanoparticles are single crystalline in nature, which have high crystallinity. The lattice spacing is measured at 0.20 nm, which is attributed to the (220) interplanar spacing of the cubic $Cu_{2-x}Se$ crystal. The inset is the corresponding FFT pattern, which further confirms the cubic structure. Fig. 4 shows a typical selected area electron diffraction (SAED) pattern taken from $Cu_{2-x}Se$ nanoparticles. The diffraction rings are responding to the (111) (220) (311) (400) (331) and (422) planes of face-centered cubic crystal structure $Cu_{2-x}Se$ (JCPDS No. 06-0680). The crystal structure of $Cu_{2-x}Se$ NCs given by SAED agrees well with that given by XRD measurements. As displayed in Fig. 2e–g, we can observe the rod-like morphology with an average length and width of 650 nm and 25 nm, respectively. Fig. 2g depicts a typical HRTEM image of an individual nanorod. Notably, the fringes in the HRTEM image are separated by 0.29 nm, in good agreement with the (200) lattice spacing of cubic $Cu_{2-x}Se$, and the oriented growth of the $Cu_{2-x}Se$ nanorods is [100] direction. Moreover, unit cell and molecular structure of face-centered cubic $Cu_{2-x}Se$ are given in Fig. 2d and Fig. 2h, respectively. The as-synthesized CuSe NCs, with hexagonal and plate-like shapes, are investigated by TEM as shown in Fig. 2i–j. Fig. 2k shows the lattice and high crystallinity of CuSe NCs. The interplanar distance of 0.34 nm corroborates the (100) lattice space of hexagonal CuSe. Obviously, CuSe nanoplates are well-crystallized and single crystals in nature. In addition, the indexed reciprocal dots inset in Fig. 2k are consistent with the hexagonal structure of CuSe with the zone axes along the direction of [0001]. The schematic model of CuSe nanoplates built according to the structure is shown in Fig. 2l.

On the basis of the above experimental results, we summarize and explain the effect of precursors on the product's shapes and structures. When $Cu(acac)_2$ and $SeC(NH_2)_2$ were used as precursors, nearly monodisperse cubic $Cu_{2-x}Se$ nanoparticles were obtained (Fig. 2a–c). On the contrary, when $Cu(Ac)_2$ was involved instead of $Cu(acac)_2$ and Se substituted for $SeC(NH_2)_2$, hexagonal plates-like NCs were obtained (Fig. 2i–k). But all the samples prepared through the approach have a relatively isotropic feature. And when $Cu(Ac)_2$ and SeO_2 were used as copper and selenium precursors, respectively, $Cu_{2-x}Se$ nanorods were generated (Fig. 2e–g). Obviously, chemical activities of the precursors could decide the product's shapes and structures. The chemical activity of $Cu(acac)_2$ is much stronger than that of $Cu(Ac)_2$, and $SeC(NH_2)_2$ has rather higher activity than Se powder.[34,35] Precursors with high reactivity tend to produce

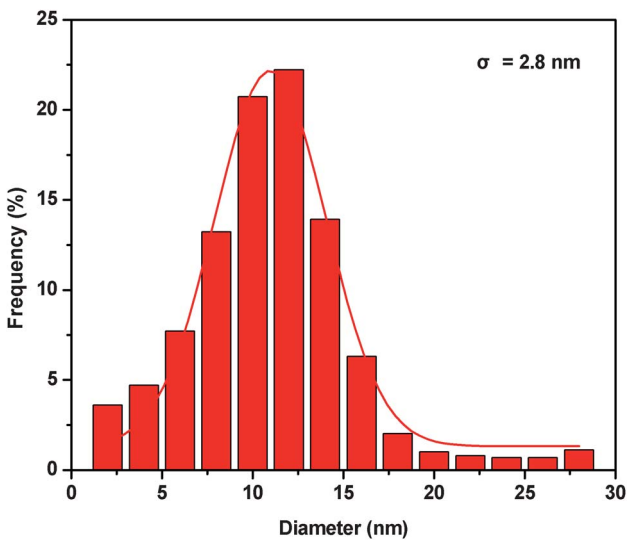

Fig. 3 Size distribution of $Cu_{2-x}Se$ nanoparticles and the standard deviation σ is about 2.8 nm.

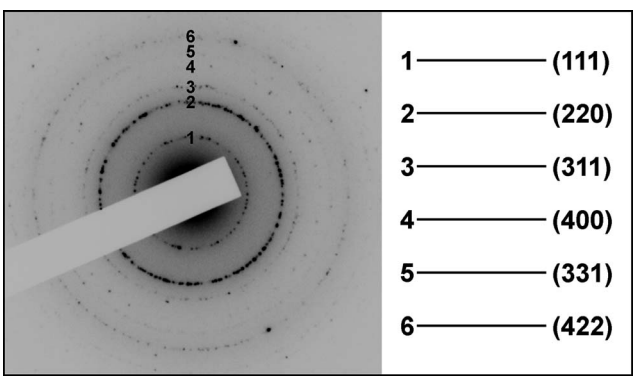

Fig. 4 Representative selected area electron diffraction (SAED) pattern of the as-prepared $Cu_{2-x}Se$ nanoparticles.

isotropic growth.[36] Just considering the size of the as-prepared nanocrystals, we can deduce that the dimension decreased with the enhanced reactivity of precursors as observed from the experimental results. The higher the reactivity of the precursors is, the smaller the size of the resulting samples. When the higher reactivity sources were involved, which leads to a high chemical potential, it would accelerate the mutual diffusion between the copper source and selenium source and further promote the reaction. As a result, the nanoscale nonstoichiometric $Cu_{2-x}Se$ was formed associated with the Ostwald ripening (OR) process.[37] However, if the less reactive precursors were employed in the solution, the chemical potential was weakened but facilitated the formation of larger CuSe with a Cu and Se molar ratio of 1 : 1. Therefore, the formation of CuSe NCs was mainly attributed to the limited dispersion between Cu and Se. Accordingly, the differences in stoichiometric compositions and crystal phase of products were mainly attributed to the diffusion effect derived from the different reactivity of precursors, which are in accord with a recent report.[26] Moreover, we can see that Se as well as $SeC(NH_2)_2$ could form Se^{2-} directly, as a result nucleation rate becomes faster and tends to isotropic growth. However, the activity of SeO_2 is much weaker than $SeC(NH_2)_2$ and Se, so that in the process of forming copper selenide NCs, SeO_2 would undergo the procedure from Se^{4+} to Se^0, and then to Se^{2-} gradually. Relatively less reactive precursors would be helpful to the growth of anisotropic nanostructures,[36] thus when SeO_2 was employed as the selenium precursor, the $Cu_{2-x}Se$ nanorods were obtained. As a consequence, the chemical activities of precursors are responsible for the shapes and structures of the as-prepared nanocrystals in our synthetic system.

To investigate the reaction time effect, we carried out the time-dependent crystal growth experiments using $Cu_{2-x}Se$ nanorods as a representative system. As shown in Fig. 5a–c, we can observe that the morphology of as-prepared products preserved the rod-like shape, only the increased size of nanorods was presented as the extension of time from 5 to 120 min. The bottom panel shown in Fig. 5d depicted the corresponding temporal XRD patterns for 5, 30 and 120 min, respectively. All the profiles with the indexed peaks can be ascribed to the cubic $Cu_{2-x}Se$. The enhanced intensity with the increasing time revealed the highly crystalline of nanorods. Unfortunately, the mutual transformation[26] between $Cu_{2-x}Se$ and CuSe was not achieved by prolonging the reaction time in the present method.

To examine the optical properties of the yielded nanocrystals, we performed room temperature ultraviolet-visible (UV-vis) absorption and photoluminescence (PL) measurements. Fig. 6 shows the normalized UV-vis absorption and PL spectra of $Cu_{2-x}Se$ nanoparticles dispersed in chloroform. The absorbent position was estimated at approximately 365 nm with the point of intersection by extrapolating the linear portions of the absorption profile. The existence of a long absorption tail is due to the dispersive scattering by the particles in the dispersion system.[38] Moreover, it is obvious that the PL spectrum provides a good reading, which represents a perfect Gaussian distribution centered at ~422 nm, and the half width at half maximum (HWHM) of emission curve is very narrow (~39 nm), indicating that the resultant $Cu_{2-x}Se$ NCs are relatively monodisperse. The optical band gap E_g of $Cu_{2-x}Se$ nanoparticles is found to be *ca.* 2.9 eV in terms of the PL peak center, which shows a blue shift

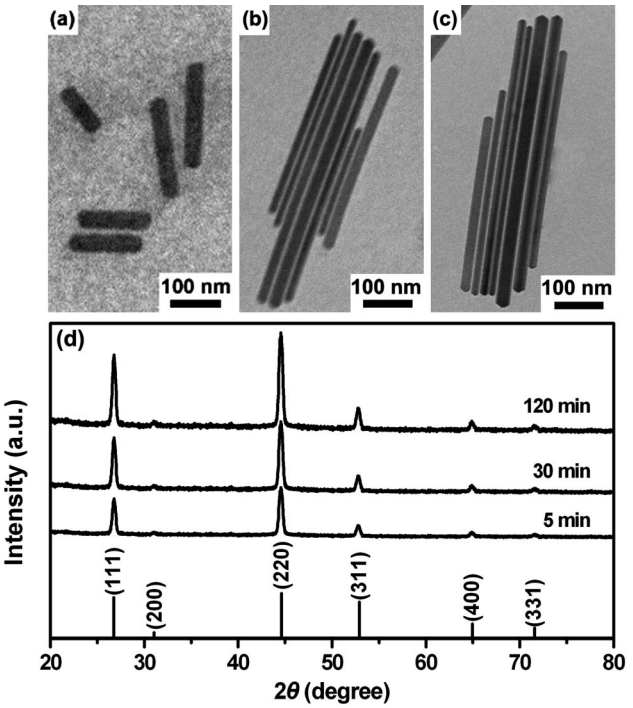

Fig. 5 Time-dependent morphology evolution (a–c) and corresponding temporal X-ray diffraction (XRD) patterns (d) using $Cu_{2-x}Se$ nanorods as a representative system for 5, 30 and 120 min, respectively.

compared to that of its bulk counterpart (2.2 eV)[39] attributing to the quantum confinement effect. The photoluminescence quantum yield of $Cu_{2-x}Se$ NCs is up to 6% by using Quinine sulfate in 0.1 M H_2SO_4 as the standard (ESI†).

In order to further evaluate the potential device applications with copper selenide NCs, we studied the electrical transport properties of the as-prepared products. Fig. 7 shows the current–voltage (*I–V*) characteristics dependent on $Cu_{2-x}Se$ nanoparticles (Fig. 7a), $Cu_{2-x}Se$ nanorods (Fig. 7b) and CuSe nanoplates (Fig. 7c), respectively. Fig. 7d illustrates the schematic of fabricated sample used for electrical measurement.

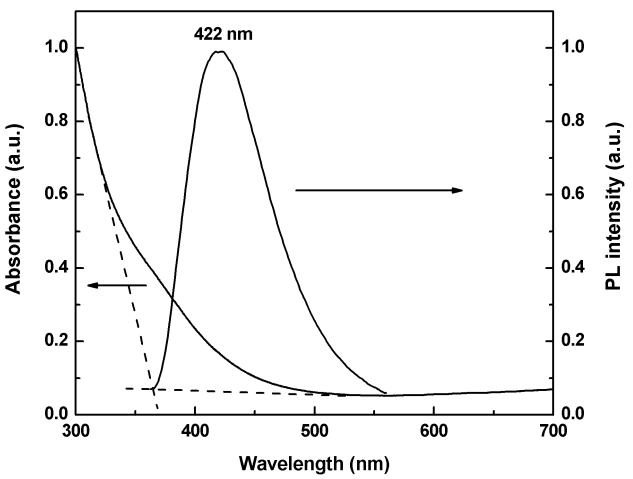

Fig. 6 Normalized ultraviolet-visible (UV-vis) absorption and photoluminescence (PL) spectra of $Cu_{2-x}Se$ nanoparticles.

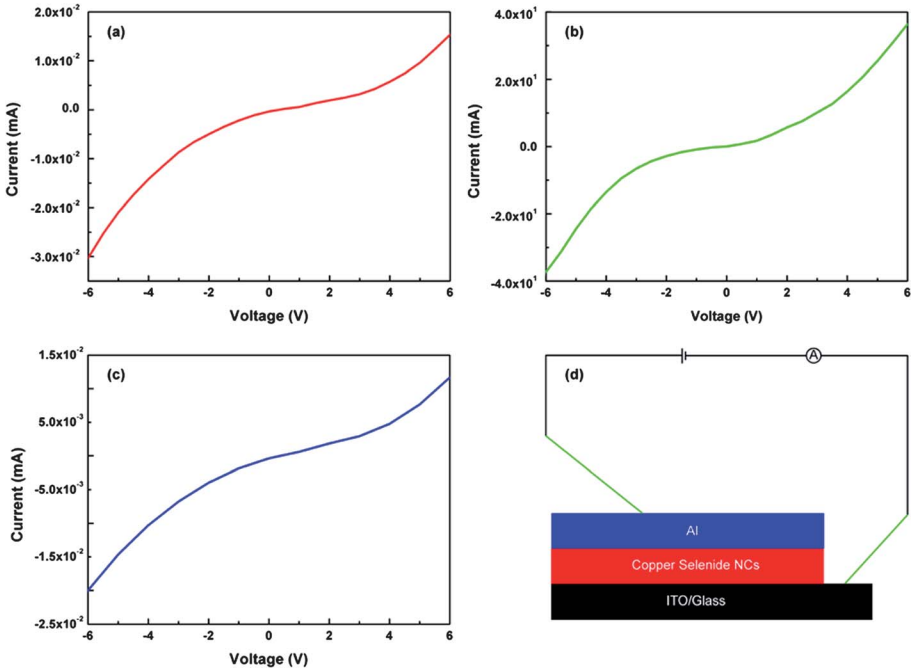

Fig. 7 Current–voltage (*I–V*) characteristics of (a) $Cu_{2-x}Se$ nanoparticles, (b) $Cu_{2-x}Se$ nanorods and (c) CuSe nanoplates; (d) shows the schematic of fabricated sample used for electrical measurement.

Obviously, the distinct nonlinear dependences with turn-on potentials denoted ranging from −6 to 6 V are observed in the *I–V* characteristics of the samples. It is indicative of a semiconductor characteristic and some degree of diode behavior. The results represented excellent electrical conductivity. Particularly, the as-synthesized $Cu_{2-x}Se$ nanorods, which indeed displayed much higher conductivity, improved nearly 3 orders of magnitude on the maximum current relative to that of the other two types. The phenomenon can be rationalized by the fact that its anisotropic rod-like shape provides a physically continuous crystal-body and a more efficient conducting pathway[40] in $Cu_{2-x}Se$ nanorods, otherwise the deleterious effects of grain-boundary recombination could be avoided thanks to the single-crystalline nature, which can be proved from the HRTEM, thus the scatter of carriers on the surface layer and on the boundaries of the nanorods would decrease[41,42] and the films with rod-like morphology outperform the granular and plate-like morphologies in achieving higher current efficiency.

Conclusions

In summary, we developed a one-pot solution route to synthesize copper selenide NCs with controllable shape and structure. The morphological features and composition of the resulting nanocrystals can be tuned upon changing the reactive precursors. It is found that the chemical activities of precursors are crucial to the morphologies and structures of the resulting products in our synthetic process. $Cu_{2-x}Se$ nanoparticles possess a distinct PL emission spectrum centered at *ca.* 422 nm and the photoluminescence quantum yield (PL QY) is up to 6%. The electric transport properties of as-prepared products ($Cu_{2-x}Se$ nanoparticles, nanorods and CuSe nanoplates) were systematically investigated and the rational reasons for the different performances depended on the morphologies were interpreted. It is worth noting that the berzelianite $Cu_{2-x}Se$ nanorods as electrical transport materials present excellent performance. The excellent performance of copper selenide NCs as electron transport materials may open new opportunities for device applications.

Acknowledgements

This work was supported by NSFC (Nos. 21073071 and 51025206) and the National Basic Research Program of China (No. 2011CB808200).

References

1 A. P. Alivisatos, *Science*, 1996, **271**, 933–937.
2 C. B. Murray, C. R. Kagan and M. G. Bawendi, *Annu. Rev. Mater. Sci.*, 2000, **30**, 545–610.
3 Y. Huang, X. F. Duan, Y. Cui, L. J. Lauhon, K.-H. Kim and C. M. Lieber, *Science*, 2001, **294**, 1313–1317.
4 Y. N. Xia, P. D. Yang, Y. G. Sun, Y. Y. Wu, B. Mayers, B. Gates, Y. D. Yin, F. Kim and H. Q. Yan, *Adv. Mater.*, 2003, **15**, 353–389.
5 J. Yang, C. Xue, S. H. Yu, J. H. Zeng and Y. T. Qian, *Angew. Chem., Int. Ed.*, 2002, **41**, 4697–4700.
6 J. Hulliger, *Angew. Chem., Int. Ed. Engl.*, 1994, **33**, 143–162.
7 S. W. Chen, R. S. Ingram, M. J. Hostetler, J. J. Pietron, R. W. Murray, T. G. Schaaff, J. T. Khoury, M. M. Alvarez and R. L. Whetten, *Science*, 1998, **280**, 2098–2101.
8 L. Y. Zhu, M. Q. Zhu, J. K. Hurst and A. D. Q. Li, *J. Am. Chem. Soc.*, 2005, **127**, 8968–8970.
9 M. Kazes, D. Y. Lewis, Y. Ebenstein, T. Mokari and U. Banin, *Adv. Mater.*, 2002, **14**, 317–321.
10 D. V. Talapin and C. B. Murray, *Science*, 2005, **310**, 86–89.
11 I. L. Medintz, H. T. Uyeda, E. R. Goldman and H. Mattoussi, *Nat. Mater.*, 2005, **4**, 435–446.
12 Q. Q. Dai, N. R. Xiao, J. J. Ning, C. Y. Li, D. M. Li, B. Zou, W. W. Yu, S. H. Kan, H. Y. Chen, B. B. Liu and G. T. Zou, *J. Phys. Chem. C*, 2008, **112**, 7567–7571.

13 Q. Q. Dai, Y. N. Wang, X. B. Li, Y. Zhang, D. J. Pellegrino, M. X. Zhao, B. Zou, J. Seo, Y. D. Wang and W. W. Yu, *ACS Nano*, 2009, **3**, 1518–1524.
14 J. J. Ning, G. J. Xiao, T. Jiang, L. Wang, Q. Q. Dai, B. Zou, B. B. Liu, Y. J. Wei, G. Chen and G. T. Zou, *CrystEngComm*, 2011, **13**, 4161–4166.
15 S. T. Lakshmikumar and A. C. Rastogi, *Sol. Energy Mater. Sol. Cells*, 1994, **32**, 7–19.
16 J. Xu, W. X. Zhang, Z. H. Yang, S. X. Ding, C. Y. Zeng, L. L. Chen, Q. Wang and S. H. Yang, *Adv. Funct. Mater.*, 2009, **19**, 1759–1766.
17 C. Lévy-Clément, M. Neumann-Spallart, S. K. Haram and K. S. V. Santhanam, *Thin Solid Films*, 1997, **302**, 12–16.
18 V. M. Bhuse, P. P. Hankare, K. M. Garadkar and A. S. Khomane, *Mater. Chem. Phys.*, 2003, **80**, 82–88.
19 J. Xu, C. S. Lee, Y. B. Tang, X. Chen, Z. H. Chen, W. J. Zhang, S. T. Lee, W. X. Zhang and Z. H. Yang, *ACS Nano*, 2010, **4**, 1845–1850.
20 M. A. Malik, P. O'Brien and N. Revaprasadu, *Adv. Mater.*, 1999, **11**, 1441–1444.
21 Y. Xie, X. W. Zheng, X. C. Jiang, J. Lu and L. Y. Zhu, *Inorg. Chem.*, 2002, **41**, 387–392.
22 X. B. Cao, C. Zhao, X. M. Lan, G. J. Gao, W. H. Qian and Y. Guo, *J. Phys. Chem. C*, 2007, **111**, 6658–6662.
23 S. Y. Zhang, C. X. Fang, Y. P. Tian, K. R. Zhu, B. K. Jin, Y. H. Shen and J. X. Yang, *Cryst. Growth Des.*, 2006, **6**, 2809–2813.
24 R. Yu, T. Ren, K. J. Sun, Z. C. Feng, G. N. Li and C. Li, *J. Phys. Chem. C*, 2009, **113**, 10833–10837.
25 W. Z. Wang, Y. Geng, P. Yan, F. Y. Liu, Y. Xie and Y. T. Qian, *J. Am. Chem. Soc.*, 1999, **121**, 4062–4063.
26 D. P. Li, Z. Zheng, Y. Lei, S. X. Ge, Y. D. Zheng, Y. G. Zhang, K. W. Wong, F. L. Yang and W. M. Lau, *CrystEngComm*, 2010, **12**, 1856–1861.
27 S. Deka, A. Genovese, Y. Zhang, K. Miszta, G. Bertoni, R. Krahne, C. Giannini and L. Manna, *J. Am. Chem. Soc.*, 2010, **132**, 8912–8914.
28 H. W. Liang, S. Liu and S. H. Yu, *Adv. Mater.*, 2010, **22**, 3925–3937.
29 X. M. Sun and Y. D. Li, *Angew. Chem., Int. Ed.*, 2004, **43**, 597–601.
30 J. J. Ning, K. K. Men, G. J. Xiao, B. Zou, L. Wang, Q. Q. Dai, B. B. Liu and G. T. Zou, *CrystEngComm*, 2010, **12**, 4275–4279.
31 J. J. Ning, G. J. Xiao, L. Wang, B. Zou, B. B. Liu and G. T. Zou, *Nanoscale*, 2011, **3**, 741–745.
32 G. J. Xiao, Q. F. Dong, Y. N. Wang, Y. M. Sui, J. J. Ning, Z. Y. Liu, W. J. Tian, B. B. Liu, G. T. Zou and B. Zou, *RSC Adv.*, 2012, **2**, 234–240.
33 H. B. Shen, H. Z. Wang, H. Yuan, L. Ma and L. S. Li, *CrystEngComm*, 2012, **14**, 555–560.
34 M. C. Gokay and L. A. Cross, *IEEE J. Quantum Electron.*, 1979, **15**, 65–66.
35 B. Mishra, P. A. Hassan, K. I. Priyadarsini and H. Mohan, *J. Phys. Chem. B*, 2005, **109**, 12718–12723.
36 Z. A. Peng and X. G. Peng, *J. Am. Chem. Soc.*, 2002, **124**, 3343–3353.
37 X. G. Peng, J. Wickham and A. P. Alivisatos, *J. Am. Chem. Soc.*, 1998, **120**, 5343–5344.
38 Y. R. Ma, L. M. Qi, J. M. Ma, H. M. Cheng and W. Shen, *Langmuir*, 2003, **19**, 9079–9085.
39 A. Hermann and L. Fabick, *J. Cryst. Growth*, 1983, **61**, 658–664.
40 J. Verilhac, G. LeBlevennec, D. Djurado, F. Rieutord, M. Chouiki, J. Travers and A. Pron, *Synth. Met.*, 2006, **156**, 815–823.
41 W. Y. Zhao, W. Y. Fu, H. B. Yang, C. J. Tian, M. H. Li, Y. X. Li, L. N. Zhang, Y. M. Sui, X. M. Zhou, H. Chen and G. T. Zou, *CrystEngComm*, 2011, **13**, 2871–2877.
42 A. Kogut, A. Mel'Nik, A. Mikolaichuk and B. Romanishin, *Russ. Phys. J.*, 1973, **16**, 1113–1116.

